Research in Pharmaceutical Sciences, October 2022; 17(5): 572-584
Received: 10-04-2022
Peer Reviewed: 29-05-2022
Revised: 04-06-2022
Accepted: 12-07-2022
Published: 08-09-2022

School of Pharmacy & Pharmaceutical Sciences
Isfahan University of Medical Sciences

Original Article

Design, synthesis, and cytotoxicity evaluation of novel indole-acylhydrazone derivatives of 4-pyridinone as potential histone deacetylase-2 inhibitors

Niloofar Naghi-Ganji[1], Lotfollah Saghaei[1], Farial Tavakoli[1], Vajihe Azimian[2], Mina Mirian[3], Hajar Sirous[4], and Mahboubeh Rostami[1,*]

[1]Department of Medicinal Chemistry, School of Pharmacy and Pharmaceutical Sciences, Isfahan University of Medical Sciences, Isfahan, I.R. Iran.
[2]Core Research Facilities (CRF), Isfahan University of Medical Science, Isfahan, I.R. Iran.
[3]Department of Biotechnology, School of Pharmacy and Pharmaceutical Sciences, Isfahan University of Medical Sciences, Isfahan, I.R. Iran.
[4]Bioinformatics Research Center, School of Pharmacy and Pharmaceutical Sciences, Isfahan University of Medical Sciences, Isfahan, I.R. Iran.

Abstract

Background and purpose: Histone deacetylation is one of the essential cellular pathways in the growth and spread of cancer, so the design of histone deacetylase (HDAC) inhibitors as anticancer agents is of great importance in pharmaceutical chemistry. Here, a series of indole acylhydrazone derivatives of 4-pyridone have been introduced as potential histone deacetylase inhibitors.
Experimental approach: Seven indole-acylhydrazone-pyridinone derivatives were synthesized *via* simple, straightforward chemical procedures. The molecular docking studies were accomplished on HDAC2 compared to panobinostat. The cytotoxicity of all derivatives was studied on MCF-7 and MDA-MB-231 breast cancer cell lines by MTT assay.
Findings / Results: Molecular docking studies supported excellent fitting to the HADC2 active site with binding energies in the range of -10 Kcal/mol for all derivatives. All compounds were tested for their cytotoxicity against MCF-7 and MDA-MB-231 cell lines; derivatives A, B, F, and G were the best candidates. The half-maximal inhibitory concentration (IC_{50}) values on MCF-7 were below 25 μg/mL and much lower than those obtained on the MDA-MB-231 cell line.
Conclusion and implications: The derivatives showed selectivity toward the MCF-7 cell line, probably due to the higher HDAC expression in the MCF-7 cell line. In this regard, debenzylated derivatives F and G showed slightly better cytotoxicity, which should be more studied in the future. Derivatives A, B, F, and G were promising for future enzymatic studies.

Keywords: Acylhydrazone; Cytotoxicity; HDAC inhibitor; Indole; Molecular docking 4-Pyridone.

INTRODUCTION

Cancer is the second leading cause of death worldwide; in 2021, new cancer cases had been predicted to be 1.9 million, and about 608,570 cancer deaths had been estimated amongst Americans (1). Anticancer drugs almost act inefficiently despite much research and effort because of different side effects and inactivation mechanisms, so cancer treatment remains a challenge for humans (2). The expression and excessive activity of different enzymes, such as histone deacetylase (HDAC), are critical factors in the pathology and development of human cancers (3).

*Corresponding author: M. Rostami
Tel: +98-3137927107, Fax: +98-3136680011
Email: m.rostami@pharm.mui.ac.ir

Access this article online

Website: http://rps.mui.ac.ir

DOI: 10.4103/1735-5362.355214

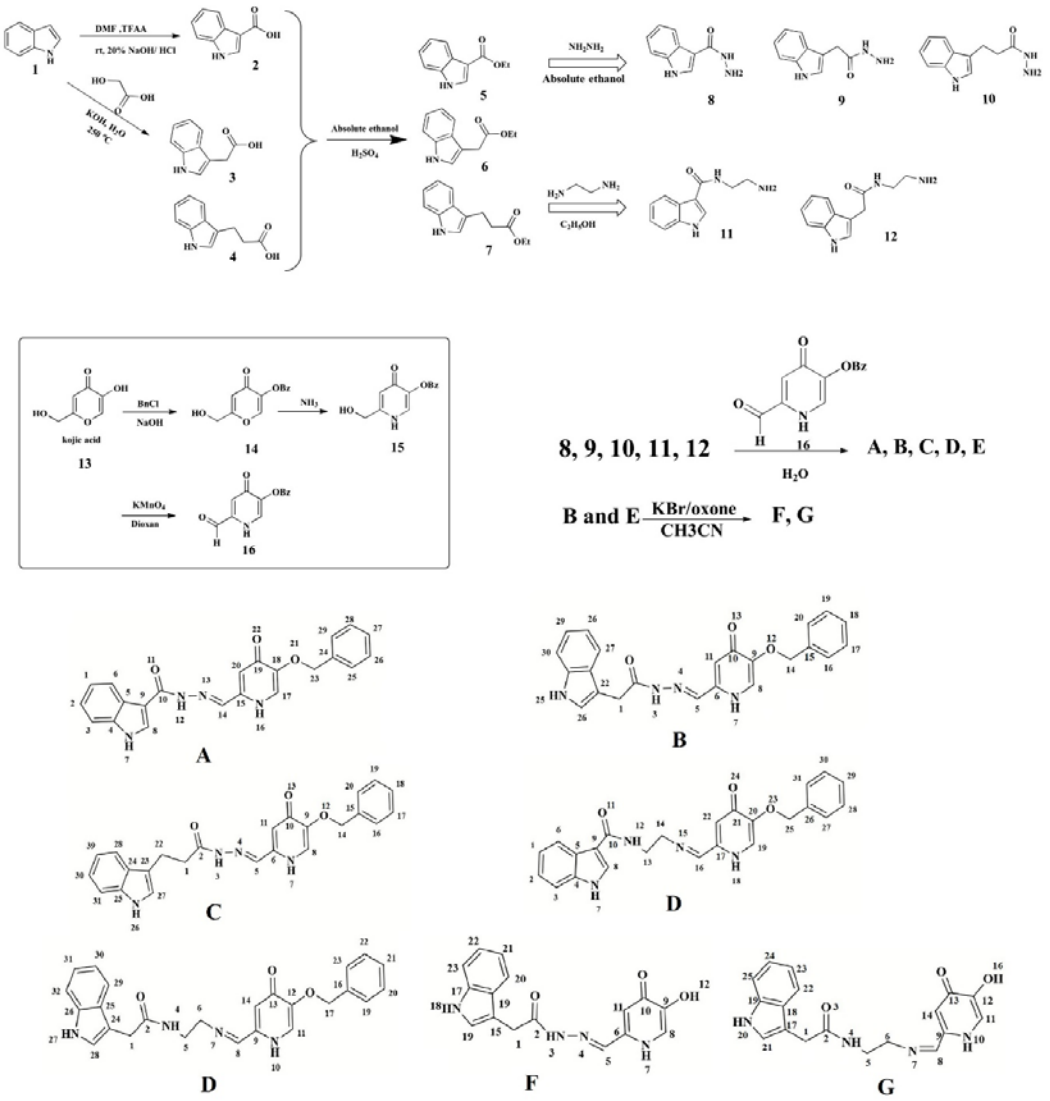

Fig. 1. General chemical procedure used for the synthesis of target derivatives A, B, C, D, E, F, and G.

HDAC plays an essential role in epigenetic regulation and changes in the level of chromatin structure. HDACs modulate the acetylation status of histones and other intracellular substrates. Their function makes the core histones entangle DNA tightly to prevent the expression of some tumor suppressor genes. Eighteen human HDACs have been discovered and categorized based on their structures and functions in four classes. HDAC classes I, II, and IV are classical zinc-dependent, while class III represents NAD^+-dependent sirtuins. Thus, the HADC enzyme has emerged as an attractive therapeutic target for developing new anticancer agents (4). So, the therapeutic potential of HDAC inhibitors has been a hotspot in cancer research (5).

Currently, some HDAC inhibitors (HDACIs) such as panobinostat, entinostat (MS-275), vorinostat (SAHA), and chidamide (HBI-8000) have been approved by FDA (6). Generally, HDAC inhibitors contain three essential motifs: cap region, zinc-binding group, and the linker, which tethers the cap region and zinc-binding group (6). Molecular designing in recent year have focused on modifying the chemical structures to interact with three critical parts in HDACs' active site.

Indole and pyridone are a significant class of heterocyclic compounds with approved anticancer activity. Different drug designs guarantee that indole (7) and pyridine (8) motifs are potential candidates for designing HDAC inhibitors.

Dai *et al.* reported a series of new SAHA derivatives with reversed amide linkers originating from substituted heteroaromatic acids (9). Among these compounds, indole amide hydroxamates were the best (10). Investigations on the different positions of the indole ring showed that 2-indole analogs were better than those substituted at other positions in potency.

Cho *et al*. reported some 2-pyridone derivatives, as histone deacetylase inhibitors, whose structures have an aromatic ring as the cap and a pyridine moiety in the core part beside the zinc-binding hydroxamate residue. They evaluated the role of the aliphatic chain and core on the different HDAC isoforms in comparison to trichostatin A (11).

Although hydroxamic acid is the most common group for binding to zinc, it has disadvantages such as structural instability, lack of isoform selection, and mutagenicity (12). New HDACI, which can bind to zinc *via* the acyl hydrazide group, has appeared recently. Li *et al*. reported structures containing the indole section that has a high selectivity for specific isoforms of HDAC compared to approved hydroxamate drugs (13).

Different structure-activity relationship (SAR) studies have been done to get the best-optimized structure; the best structure resulting from SAR has been chidamide, which was approved in 2015 by the China Food and Drug Administration as a specific inhibitor of HDAC1 for the treatment of relapsed / refractory peripheral T cell lymphoma (14). The interactions created by the cap and linker groups with different kinds of functionality can regulate selectivity, potency, pharmacokinetic properties, and toxicity and contribute to the overall performance of the HADC inhibitor (12).

Therefore, in this study, to introduce a new class of HDAC inhibitors, indole acyl hydrazine derivatives of 4-pyridone were introduced for the first time. Their initial cytotoxic effects on two MCF-7 and MDA-MB-231 breast cancer cell lines were evaluated. Molecular docking studies have been performed to confirm the initial structure-enzyme interactions on HDAC2. The structure of the designed compounds and synthesis procedures is presented in Fig. 1.

MATERIALS AND METHODS

Materials and instruments

All chemicals were purchased from Merck and Sigma-Aldrich chemical companies and were used without further purification. Thin-layer chromatography (TLC) was accomplished on Merck silica gel (60F254) sheets. Proton and carbon-13 nuclear magnetic resonance (1H NMR and 13C NMR) spectra were recorded in either deuterated dimethyl sulfoxide (DMSO-d_6) or CDCl3 solvents on Bruker 400 MHz spectrometer (Germany) using tetramethylsilane (TMS) as an internal reference. Infrared (IR) spectra were recorded as KBr pellets on a WQF-510 Fourier-transform (FT)-IR spectrophotometer (China). Elemental analysis was carried out using an elemental analyzer for CHNS (Perkin Elmer-2400, USA). Melting points were determined using electrothermal 9200 melting point apparatus (England).

Synthesis of 1H-indole-3-carboxylic acid (2)

The indole-3-carboxylic acid was synthesized based on the available procedure (15). Briefly, a 30% w/v solution of indole in dimethylformamide was cooled, and trifluoroacetic anhydride (1.2 equivalents) was added dropwise under stirring. The reaction was continued for 3 h at room temperature; at the end, the mixture was poured into water (10 mL). The product was filtered, washed with water, and dried under a vacuum at 80 °C. The product was refluxed in NaOH (20% w/w) for 1 h; the solution was cooled and acidified with HCl (37%) to precipitate indole-3-carboxylic acid. Precipitates were filtered and washed with water, dried at 100 °C, and subsequently recrystallized from acetone/water to get indole-3-carboxylic acid with an overall yield of 85% and a decomposition temperature of 236-238 °C.

Synthesis of 2-(1H-indol-3-yl)acetic acid (3)

To a mixture of indole (351g, 3 mol) and KOH (270 g, 85%) in a stainless-steel autoclave vessel, glycolic acid (360 g, 3.3 mol) was added portion-wise. The autoclave was closed and heated at 250 °C for 20 h. The reaction mixture was cooled to room temperature, water (200 mL) was added, and heated at 100 °C to dissolve the potassium salt of indole-3-acetic acid. After cooling, ether (500 mL) was added, and the aqueous solution was isolated cooled and acidified with HCl (37%). The precipitates were collected by filtration, washed with water, and dried under a vacuum. The product was recrystallized from water to get off-white powder with a 90% yield and a melting point of 164-166 °C (16).

Synthesis of ester derivatives 5-7

To a methanolic solution of indole acids (Fig. 1) comprising 2, 3, and 4 (1 g), 1 mL of concentrated H_2SO_4 was added, and the mixture was refluxed for about 12-16 h to complete the esterification. After completing the reaction and cooling the mixture, methanol was removed by a rotary evaporator. The residue was slowly neutralized by adding aq. NaHCO3 (20 % w/v) and then extracted with ethyl acetate. The ethyl acetate phase was dried on $MgSO_4$ and evaporated using a rotary evaporator; the crude product was further purified by flash chromatography if needed to get pure 5, 6, and 7 in an average yield of 90% (17).

Synthesis of indole acylhydrazone derivatives 8-10

Briefly, a mixture of appropriate ester (1 mmol) and hydrazine hydrate (2 mmol) in ethanol (10 mL) was refluxed for 3-5 h. the reaction mixture was cooled. Precipitates were filtered, washed with a small amount of water, dried, and finally recrystallized from ethanol to get pure acylhydrazone derivatives 8-10 (Fig. 1) with an average yield of 85% (18).

Synthesis of N-(2-aminoethyl) indole amide derivatives 11 and 12

A mixture of appropriate indole carboxylic acid ester (5 or 6, 2 mmol) (Fig. 1) and ethylenediamine (3 mL) was heated at 100-120 °C for five days. Excess ethylenediamine was removed by rotary evaporator; ether was added to the residue to get pale yellow powder. The crude product was dried under a vacuum to get desired pure products with an average yield of around 60% (19).

Synthesis of 5-(benzyloxy)-4-oxo-1,4-dihydropyridine-2-carbaldehyde (16)

Compound 16 was synthesized based on previous reports in three-step successive reactions from kojic acid (compound 13, Fig. 1). At first, 5-OH of kojic acid was benzylated in the presence of KOH and benzyl chloride in methanolic solution to give 14 (20). In the next step, compound 14 was refluxed in ethanolic ammonia overnight to get compound 15 (21). Finally, compound 15 was dissolved in CH2Cl2, activated MnO2 was added in excess, and the mixture was vigorously stirred at around 35 °C for three days. The reaction progress was checked by TLC, the mixture was filtered, and the filtrate was concentrated to get compound 16 with an overall yield of 72% (22).

Synthesis of final derivatives A-E

An equimolar mixture of 16 (Fig. 1) and desired amine derivatives (A-E) was refluxed in CHCl3/ethanol mixture (8:2). The reaction progress was monitored by TLC; upon completion, the solvent was removed by rotary evaporation. The crude product was recrystallized from ethyl acetate or ethanol to get pure A, B, C, D, and E with an average yield of 86% (23).

Synthesis of final derivatives F and G

To a solution B or E (0.5 mmol) in 25 mL of cooled dried CH_2Cl_2 under an N_2 atmosphere, BCl_3 (1 M in DCM, 2 mL) was added under stirring; the reaction was continued at room temperature for 6 h. Methanol (10 mL) was added to neutralize the excess BCl_3 and stirred for another half an hour at room temperature. Finally, the solvent was removed under vacuum, and the product was recrystallized in ethanol to get pure F and G with an average yield of 72% (20).

Cytotoxicity assessment

200 µL of cell suspension (MCF-7 and MDA-MB-231) with a 4×10^4 cells/mL seeding density were seeded in 96-well plates. The plates were incubated at 37 °C with 5% CO_2 overnight to allow cell attachment. Serially diluted solutions (5, 10, 25, and 50 µg/mL) of final synthesized derivatives were added into the appropriate wells in three replicates for each concentration; untreated cells (0 µg/mL) were used as a negative control. In this study, doxorubicin was used as a positive control to ensure the viability of cancer cells and their response to treatment groups. To get the best results, 48 h of incubation was selected for assay on both MDA-MB-231 and MCF-7 cells. After incubation, 20 µL of MTT solution was added to the wells, and the plates were incubated for a further 4 h. The medium of each well was carefully removed; DMSO (150 µL) was added to the wells to dissolve the purple formazan crystals, and incubation was continued for 4 h. The optical density (OD) of formazan was proportional to the number of surviving cells and was read at 490 nm wavelength. Dose-response curves (percentage of cell survival versus concentration) were generated using linear regression interpolation analysis to obtain the IC_{50}s of MDA-MB-231 and MCF-7 cells. All experiments were repeated three times, and the average was used as the result. The cell survival percent was calculated according to the following equation (24):

$$Cell\ viability\ (\%) = \frac{\text{Abs (sample)} - \text{Abs (blank)}}{\text{Abs (negative control)} - \text{Abs (blank)}} \times 100$$

Docking studies

Crystal structure of HDAC2-inhibitor complex was retrieved from Protein Data Bank (PDB ID: 4LY1 with a resolution of 1.57 Å). The inhibitor and water molecules were removed from the complex. HDAC2 structure was in asymmetric homotrimer form, so a monomer was used for the study. The Swiss Model server was applied to repair the chain breaks in the structure (25). The chemoinformatics tool ChemDraw Ultra was applied to design desired compounds. The 3D structures of seven designed compounds were obtained in protein data format (PDB) using Accelrys Discovery Studio 4.0 Visualizer (DS 4.0, 133 Accelrys Software Inc., San Diego, CA, USA). Physicochemical properties of the seven designed compounds, including molecular weight (MW), LogP calculated with XLOGP3 method, LogD at physiological PH (7.4), LogSw, hydrogen-bond donor (HBD), and hydrogen-bond acceptor (HBA) were investigated using the FAF-Drugs4 web server (26). The 3D structures of the protein and designed compounds were converted into an AutoDock-compatible file format (pdbqt) using OpenBabel (Pittsburgh, PA, USA) (27). Virtual screening of the designed compounds against the HDAC2 protein was performed in comparison to Panobinostat using AutoDock Vina (28) in the PyRx v0.8 (The Scripps Research Institute, La Jolla, CA, USA) (29). All the prepared structures and Panobinostat were targeted against the HDAC2 protein in a local docking manner. The search was performed with the Lamarckian genetic algorithm and an empirical free energy scoring function. The molecular docking was performed inside a grid box (X-, Y- and Z-axes), with dimensions of (15.608 Å × -19.609 Å × 3.734 Å), respectively. The analysis results for different protein-ligand complexes were determined for the predicted binding energy. Then, the docked complexes were clustered and compared by the best-ranked ligand with a root-mean-square deviation (RMSD) value of 2.0 Å. Nine different poses were generated for each ligand, and the poses with the lowest energy were selected for further analysis. The binding poses and atomic interactions of the docked complexes with the lowest binding affinity were visualized and analyzed using Discovery Studio.

Statistical analysis

One-way ANOVA was implemented using SPSS software to evaluate the differences between the groups. Furthermore, for checking the differences between two groups' paired-wise comparison t-test and for the differences among more than two groups, the LSD post hoc test was used. *P*-values lower than 0.05 were considered significant.

RESULTS

The chemical structure of compounds A, B, C, D, E, F, and G was studied and confirmed using IR, NMR, and CHNS spectroscopy. The results are presented below. The atom-assigned numbers are presented in Fig. 1. Furthermore, 1H NMR and 13C NMR spectra of compound A as the representative have been provided in Fig. 2.

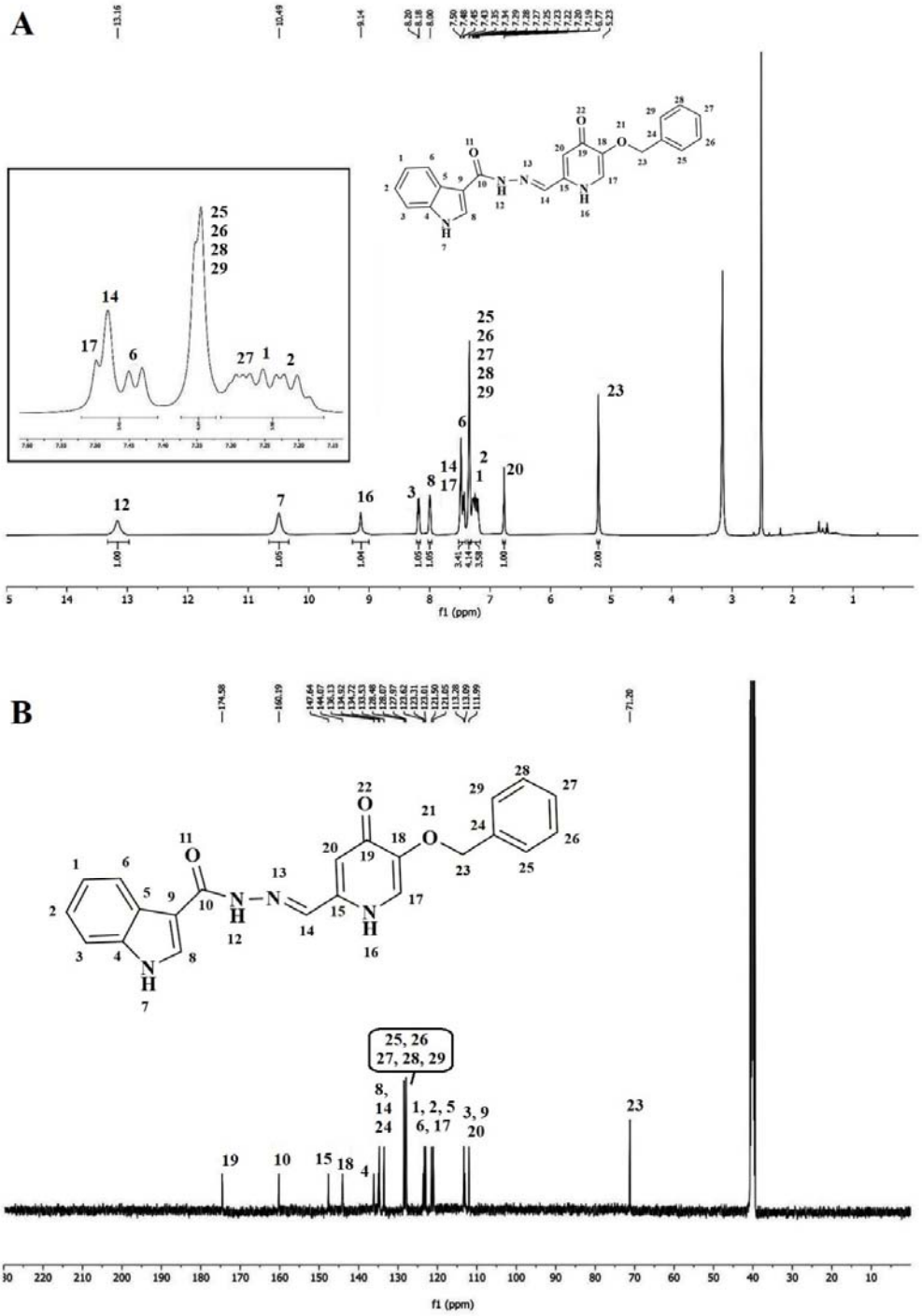

Fi. 2. (A) 1H NMR and (B) 13C NMR spectra of compound A (deuterated dimethyl sulfoxide, 400 MHz

(E)-N'- ((5-(benzyloxy)-4- oxo-1 ,4-dihydro-pyridin-2-yl) methylene)-1H-indole-3-carbo-hydrazide (A)

Melting point: 232-234 °C; FTIR (KBr): υ (cm-1): 3279 (N-H str.), 3060 (C-H str, C=C), 2974, 2866 (C-H str. aliphatic), 1653 (C=O str.), 1617 (C=O str.), 1535, 1483, 1453, 1390, 1419, 1271, 1237, 1166, 1080, 1025; 1H NMR (400 MHz, DMSO) δ (ppm): 13.16 (S, 1H, H12), 10.49 (s, 1H, H7), 9.14 (s, 1H, H16), 8.20 (d, *J* = 8.0 Hz, 1H, H3), 8.00 (s, 1H, H8), 7.50-7.43 (m, 3H, H17,14,6), 7.35-7.19 (m, 7H, H1, 2, 25, 26, 27, 28, 29), 6.77 (s, 1H, H20), 5.23 (s, 2H, H23); 13C NMR (100 MHz, DMSO) δ (ppm) 174.58 (C19), 160.19 (C10), 147.64, 144.07, 136.13, 134.92, 134.72, 133.53, 128.48, 128.07, 127.97, 123.62, 123.31, 123.01, 121.50, 121.05, 113.28, 113.09, 111.99,71.20 (C23); elemental analysis for $C_{22}H_{18}N_4O_3$, theoretical: C, 68.38; H, 4.70; N, 14.50, found: C, 68.42; H, 4.75; N, 14.46.

(E)-N'-((5-(benzyloxy)-1,4-dihydropyridin-2-yl) methylene)-2- (1H-indol-3-yl) aceto-hydrazide (B):

Melting point: 229-231 °C FTIR (KBr): υ (cm-1): 3295 (N-H str.), 3030 (C-H str. C=C), 2914 (C-H str. aliphatic), 1641 (C=O str.), 1595 (N-H def. or ring vibration), 1541, 1508, 1383, 1360, 1269, 1198, 1146, 1093, 1074; 1H NMR (400 MHz, DMSO) δ (ppm): 11.77 (S, 1H, H3), 10.90 (S, 1H, H25), 9.15 (s, 1H, H7), 7.60 (d, *J* = 8.0 Hz, 1H, H27), 7.49 (d, *J* = 8.0 Hz, 2H, H5,8), 7.34-7.24 (m, 5H, H16, 17, 19, 20, 30), 7.22-6.77 (m, 4H, H18, 26, 29, 28), 5.19 (s, 2H, H14), 3.97 (s, 2H, H1); elemental analysis for $C_{23}H_{20}N_4O_3$, theoretical: C, 68.99; H, 5.03; N, 13.99, found: C, 69.09; H, 5.10; N, 13.90.

(E)- N'- ((5-(benzyloxy)-4-oxo-1 ,4-dihydro-pyridin-2- yl)methylene)-3- (1H-indol-3-yl) propanehydrazide (C)

Melting point: 207-209 °C; FTIR (KBr): υ (cm^{-1}) 3292(N-H str.), 3253(N-H str.), 3055 (C-H str. C=C), 2925 (C-H str. aliphatic), 1671 (C=O str.), 1616, 1549, 1518, 1439, 1408, 1371, 1313, 1248, 1161, 1122; 1H NMR (400 MHz, DMSO) δ (ppm): 11.57 (S, 1H, H3), 9.95 (s, 1H, H26), 9.13 (s, 1H, H7), 7.61-7.49 (m, 3H, H28, 5, 8), 7.34-7.16 (m, 6H, H16, 17, 18, 19, 20, 31), 7.12-6.77 (m, 4H, H3, 27, 29, 11), 5.23 (s, 2H, H14), 3.30 (s, 2H, H1), 2.81 (s, 2H, H22); 13C NMR (100 MHz, DMSO) δ (ppm) 174.58 (C10), 170.16 (C2), 147.66 (C6), 144.07 (C9), 136.26, 134.92, 134.39, 128.48, 128.07, 127.97, 127.07, 123.01, 122.118, 121.75, 118.67, 118.36, 115.55, 113.28, 111.26, 71.20 (C14), 33.23 (C1), 21.53 (C22); elemental analysis for $C_{24}H_{22}N_4O_3$, theoretical: C, 69.55; H, 5.35; N, 13.52, found: C, 69.60; H, 5.39; N, 13.47.

N- (2- (((5-(benzyloxy)-4-oxo-1,4-dihydr-opyridin-2-yl) methylene)amino)ethyl)-1H-indole-3-carboxamide (D)

Melting point: 195-197 °C; FTIR (KBr): υ (cm^{-1}) 3282 (N-H str.), 3030 (C-H str. C=C), 2925, 2833 (C-H str. aliphatic), 1624 (C=O str.), 1562, 1453, 1358, 1275, 1232, 1178; 1H NMR (400 MHz, DMSO) δ (ppm): 10.75 (S, 1H, H7), 8.67 (s, 1H, H18), 8.42 (s, 1H, H12), 8.17 (d, *J* = 8.00 Hz, 1H, H3), 7.90 (s, 1H, H8), 7.89 (s, 1H, H16), 7.44-7.29 (m, 4H, H27, 28, 30, 31), 7.28-7.19 (m, 3H, H29, 1, 2), 6.73 (s, 1H, H22), 5.19 (s, 2H, H25), 3.75 (s, 2H, H14), 3.63 (s, 2H, H13); elemental analysis for $C_{24}H_{22}N_4O_3$, theoretical: C, 69.21; H, 5.81; N, 13.45, found: C, 69.30; H, 5.92; N, 13.41.

N- (2- (((5-(benzyloxy)-4-oxo-1,4-dihydro-pyridin-2-yl)methylene)amino)ethyl)-2-(1H-indol-3-yl)acetamide (E)

Melting point: 189-191 °C; FTIR (KBr): υ (cm^{-1}): 3290 (N-H str.), 3070 (C-H str. C=C), 3042 (C-H str., C=C), 2935, (C-H str. aliphatic), 2873 (C-H str. aliphatic), 1629 (C=O), 1616, 1580, 1523, 1356, 1269, 1201, 1141; 1H NMR (400 MHz, DMSO) δ (ppm): 10.89 (S, 1H, H27), 8.68 (s, 1H, H10), 8.03 (s, 2H, H4), 7.78 (s, 1H, H8), 7.61 (d, *J* = 8.0 Hz,1H, H29), 7.45 (d, *J* = 4.00 Hz, 1H, H11), 5.23 (s, 2H, H17), 3.81 (s, 2H, H1), 3.63 (s, 2H, H6), 3.55 (s, 2H, H5); 13C NMR (100 MHz, DMSO) δ (ppm) 174.71 (C13), 171.15 (C2), 151.72 (C8), 144.85, 144.11, 146.06, 134.92, 128.48, 128.07, 127.97, 124.03, 122.19, 121.71, 118.70, 118.46, 115.11, 111.12, 110.06, 71.20(C17), 53.57 (C6), 43.38 (C5), 33.48 (C1); elemental analysis for $C_{25}H_{24}N_4O_3$, theoretical: C, 70.08; H, 5.65; N, 13.08, found: C, 70.15; H, 5.72; N, 12.94.

(E)-N'-((5-hydroxy-4-oxo-1,4-dihydropyridin-2-yl)methylene)-2-(1H-indol-3-yl)acetohydrazide (F)

Melting point > 190 °C; FTIR (KBr): υ (cm^{-1}) 3363 (O-H str.), 3281 (N-H str.), 3068 (C-H str. C=C), 2927 (C-H str. aliphatic), 1667 (C=O, str.), 1614, 1593, 1578, 1568; 1H NMR

(400 MHz, DMSO) δ (ppm): 11.77 (S, 1H, H3), 10.91 (s, 1H, H18), 10.46 (s, 1H, H7), 10.17 (s, 1H, H12), 7.81 (d, *J* = 4.16 Hz, 1H, H8), 7.61 (d, *J* = 8.00, 1H, H20), 7.49 (s, 1H, H5), 7.36 (d, *J* = 8.00 Hz, 1H, H23), 7.24-7.08 (m, 3H, H19, 21, 22), 6.66 (s, 1H, H11) 3.68 (s, 2H, H1); elemental analysis for $C_{16}H_{14}N_4O_3$, theoretical: C, 61.93; H, 4.55; N, 18.06, found: C, 61.98; H, 4.61; N, 17.96.

N-(2-(((5-hydroxy-4-oxo-1,4-dihydropyridin-2-yl)methylene)amino)ethyl)-2-(1H-indol-3-yl)acetamide (G)

Melting point > 230 °C; FTIR (KBr): υ (cm^{-1}): 3364 (O-H str.), 3280 (N-H str.), 3077 (CH str. C=C), 2929 (C-H str. aliphatic), 1666 (C=O, str.), 1610, 1596, 1576, 1564; 1H NMR (400 MHz, DMSO) δ (ppm): 10.90 (d, *J* = 8.0 Hz, 1H, H20), 10.17 (s, 1H, H10), 8.03 (s, 1H, H4), 7.82(d, *J* = 8.0 Hz, 1H, H11), 7.77 (s, 1H, H8), 7.61 (d, *J* = 8.0 Hz, 1H, H25), 7.21-7.08 (m, 3H, H21, 24, 23), 6.58 (s, 1H, H14), 3.81 (s, 2H, H1), 3.60 (s, 2H, H6), 3.45 (s, 2H, H5); 13C NMR (100 MHz, DMSO) δ (ppm): 172.67 (C13), 171.25 (C2), 152.01 (C8), 145.04 (C9), 142.07, 136.6, 128.65, 124.02, 121.71, 118.70, 118.46, 111.70, 111.12, 110.06, 53.57 (C6), 40.14 (C5), 33.48 (C1); elemental analysis for $C_{18}H_{18}N_4O_3$, theoretical: C, 63.89; H, 5.36; N, 16.56, found: C, 63.92; H, 5.39; N, 16.53.

Cytotoxicity

The cytotoxic effect of compounds A, B, C, D, E, F, and G in a primary screening with concentrations of 5, 10, 25, and 50 µg/mL was investigated and the results have been shown in Fig. 3. In addition, the IC_{50} values of MCF7 and MDA-MB-231 cells have been summarized in Table 1.

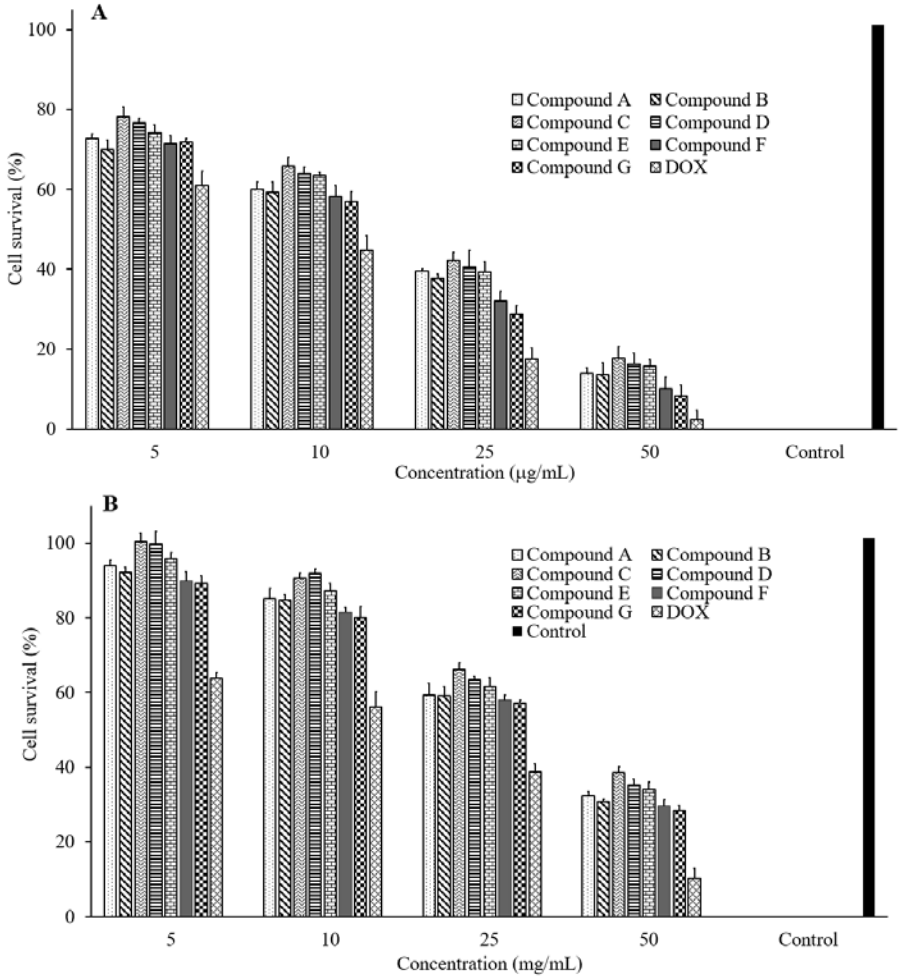

Fig. 3. Cytotoxicity profile of synthesized derivatives at different concentrations on (A) MCF-7 and (B) MDA-MB-231 cell lines compared to the DOX. The IC_{50} values are the means of three experiments. $^{*}P < 0.05$ Indicates significant differences in comparison with the negative control group; $^{\#}P < 0.05$ shows significant differences between compounds C, D, and E with compounds A, B, F, and G. DOX, Doxorubicin.

Table 1. IC_{50} values for different derivatives on MCF-7 and MDA-MB-231 cell lines.

Compounds	IC_{50} on MCF-7 cells (µg/mL)	IC_{50} on MDA-MB-231 cells (µg/mL)
A	19.74 ± 0.26	35.48 ± 0.76
B	18.55 ± 0.59	34.66 ± 0.39
C	23.28 ± 0.31	40.15 ± 0.63
D	22.07 ± 0.47	38.15 ± 0.41
E	21.09 ± 0.58	36.93 ± 0.59
F	17.17 ± 0.63	33.55 ± 0.31
G	16.20 ± 0.77	32.7 ± 0.69
Doxorubicin	8.46 ± 0.63	15.89 ± 0.83

Table 2. Binding energy and number of predicted interactions of top-scoring poses of docked compounds with HDAC2 (PDB: 4LY1).

Compounds	Binding energy (Kcal/mol)	Number of residues*
Panobinostat	-9.4	4
A	-10.2	8
B	-9.5	9
C	-9.8	9
D	-10.0	8
E	-9.7	7
F	-8.9	10
G	-9.4	7

HDAC, Histone deacetylase inhibitors; * displays the number of HAC2 active site residues interacting with compounds.

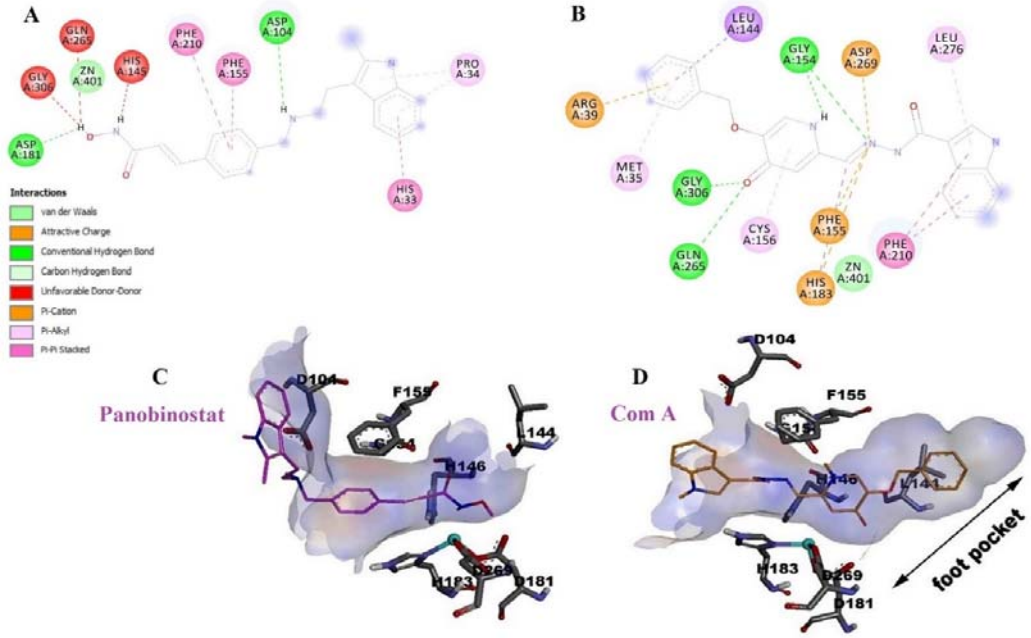

Fig. 4. 2D plots of predicted interactions between HDAC2 active site and compound A. (A) Panobinostat and (B)compound A in interaction with HDAC2; (C) close view of the panobinostat and (D) compound A binding mode to the active site of HDAC2. HDAC, Histone deacetylase inhibitors.

Ducking studies

Free binding energy values in Kcal/mol and the number of favorable interactions with key amino acid residues in the enzyme's active site for studied compounds have been provided in Table 2. Predicted interactions between HDAC2 active site and compound A compared to panobinostat in different representation modes have presented in Fig. 4.

DISCUSSION

Histone deacetylase inhibitors, especially class 1, 2, and 4 inhibitors, as mentioned earlier, have three key components in the structure (30), cap, linker, and zinc bonding section. In many designs in recent years, zinc bonding has often been the target of the design (6). All three parts of cap, linker, and zinc bonding moiety have been our focus in this study. The indole part and the acylhydrazone group were selected due to structural and bioisosteric similarity with the cap part in panobinostat. The 3-hydroxy-4-pyridinone part was initially considered a zinc-chelating moiety. There are many reliable reports about 3-hydroxy-4-pyridinone structures and their ability to chelate various divalent and trivalent metals (31). It seemed that, according to the existing studies, this structural part could be a suitable candidate for the zinc-binding part in the new design. Preliminary studies predicted that one of the Schiff base-amine or oxy-ketone moieties of the 3-hydroxy-4-pyridone ring could be a chelating agent for zinc.

The desired compounds (A, B, C, D, E, F, and G) were synthesized starting from indole acid derivatives (2, 3, and 4) based on the procedure provided in Fig. 1. Indole acids 2 and 3 were synthesized from indole using available procedures, and their melting point, IR, and 1H NMR spectra were compared with the reported cases, and indole acid 4 was purchased. The chemical structures of the synthesized compounds were confirmed by FTIR, 1H NMR, 13C NMR, and CHNS. The presence of characteristic structural signals for the indole, hydrazide, and pyridone segments in the final derivatives spectra with correct integrals and the agreement of theoretical and experimental results in the CHNS analysis confirmed the structural validity.

In this study, two breast cancer cell lines MCF-7 and MDA-MB-231 were used to determine the cytotoxicity of the synthesized compounds. Many studies point to the role of HDAC in physiology and tumorigenesis in the breast. Some studies have specifically considered the high expression of HDACs 1, 3, and 6 (32). Some studies are available that report HDACIs as promising agents for breast cancer therapy (33).

As shown in Fig. 3, the cytotoxicity effect of the synthesized compounds showed a concentration-dependent trend in both cell lines. IC_{50}s on the MCF7 cell line are estimated to be below 25 µg/mL and in the MDA-MB-231 cell line, of course, are in the range of 25 and 50 µg/mL. The obtained IC_{50}s on the MCF-7 cell line were in the range of those reported by Ding *et al.* for coumarin-based N-hydroxycinnamamide derivatives (34). There is no significant difference between the results of compounds A, B, F, and G on one hand and compounds C, D, and E on the other hand in both cell lines. Among the different compounds, compounds C, D, and E showed less cytotoxic effects in almost all concentrations, and according to IC_{50} results (Fig. 3), these three compounds have the highest IC_{50}. However, there is a significant difference between the cytotoxicity results in each of A, B, G, and F with each of C, D, and E compounds.

Although this conclusion is somewhat immature, we can point to the longer length of the aliphatic chain in these two compounds, which seems to have had an overall negative effect on the toxicity of these compounds. Bingul *et al*. (35) have also reported a negative effect of increasing chain length in acylhydrazone derivatives similar to ours.

Another exciting result regarding cytotoxicity belongs to the de-benzylated compounds of F and G. However, neither of these compounds directly interacted with zinc in the evaluation of molecular docking; it seems to show mild better toxicity effects (lower IC_{50} values, Fig. 3). However, the observed differences compared to A and B are not significant.

Finally, the cytotoxicity effects of all compounds are less in the MDA-MB-231 cell line, which can be generally attributed to the lower sensitivity of this cell line or the lower level of histone deacetylase expression in this cell line. Margueron *et al.* (36) have previously shown that HDACIs are more sensitive to MCF7 cell line than MDAMB231 cell line; in other words, HDACIs seem effectively inhibit cell proliferation in estrogen receptor-positive human breast cancer cells (MCF-7) (37). While reaffirming this finding, this study can create apparent horizons for expanding research in this category of compounds.

Computer-aided drug designs, especially structure-based virtual screening, play an essential role in the drug discovery process and development of lead compounds and reduce the experimental time and cost. Molecular docking as a critical tool is applied widely to build, visualize, and analyze molecular structures at the atomic level (38). A molecular docking technique has been employed to investigate the binding affinity and binding modes of designed compounds and panobinostat in complex with HDAC2.

Panobinostat displayed the binding affinity of -9.4 kcal/mol and covered 4 active site residues, including His 145, Phe 155, Asp 181, and Phe 210 (Fig. 4). Among the designed compounds, compound A (compared to panobinostat) showed the highest binding affinity (-10.2 kcal/mol) and covered more residues of HDAC2 active site, including Met 35, Leu 144, Gly 154, Phe 155, His 183, Phe 210, Asp 269 and Leu 276 (Fig. 4). In addition, compounds A, B, C, D, and E displayed higher binding affinities than panobinostat (-9.5, -9.8, -10.0, and -9.7 kcal/mol), respectively, and covered the identical residues mentioned above. Finally, compound F displayed the lowest binding affinity of -8.9 kcal/mol, in the range of panobinostat (Table 3). Physicochemical properties of the designed compounds were calculated by applying the FAF-Drugs4 web server (26). All the designed compounds were accepted as drug candidates based on calculated physicochemical properties. The docking results suggested that compound A could be considered a selective inhibitor for HDAC2. Compound A covers more residues of the active site, particularly the hydrophobic tunnel and foot pocket key residues. Compound A enters the active site by its benzyl group, reaches the foot pocket depth, and makes hydrophobic interactions with foot pocket key residues, Met 35 and Leu 144 (Fig. 4D). The aromatic indole group at the other end of the molecule fits at the pocket entrance and forms two π-π stacking interactions with Phe 210 and hydrophobic interaction with Leu 276. The length of the linker appears to be optimal for spanning the lipophilic tunnel and foot pocket, allowing interactions, particularly hydrogen bonds and electrostatic bonds, with the critical residues. There are five hydrogen bonds in HDAC2-compound A complex, three of them are made between the oxygen atom of the pyridone group and residues, Gln 265 side chain and the amino group of Gly 306, and 2 other hydrogen bonds are formed between the carboxyl group of Gly 154 and the NH group of pyridone and the nitrogen atom of hydrazide group (Fig. 4). In addition, the nitrogen atom of hydrazide is involved in electrostatic interactions with the side chains of His 183 and Asp 269 (Fig. 4). When the panobinostat enters the binding pocket, the hydroxamate group at the end of the molecule structure binds to the catalytic domain in the middle of the lipophilic tube, and it tends to show fast binding kinetics (39).

CONCLUSION

In this study, to find some HDACIs, a new class of indole acyl hydrazone derivatives from 4-pyridinone were introduced, and their initial cytotoxicity was studied on MCF-7 and MDA-MB-231 cell lines. The results showed that there were concentration-dependent effects in both cell lines. Except for those derivatives whose aliphatic chain length was longer in the middle of the structure, the other derivatives showed approximately similar cytotoxic effects. IC_{50} values in the MCF7 cell line (about 20 μg/mL) are significantly lower than in the MDA-MB-231 cell line (30-40 μg/mL), which could be attributed to the higher expression of HDAC enzymes in the MCF7 cell line. The cytotoxicity of debenzylated derivatives (F and G) was slightly higher than benzylated derivatives. Molecular docking studies indicated that the designed structures were well fitted in enzyme active site with binding energy better than panobinostat. Our preliminary results indicate the possible effects of these compounds as HDACIs, which will be evaluated in future studies.

Acknowledgments

This work was financially supported by the Research Vice Chancellery of Isfahan University of Medical Sciences, I.R. Iran through thesis No. 397789.

Conflicts of interest statements

The authors declared no conflicts of interest in this study.

Authors' contribution

M. Rostami contributed to the conception and design of the work, conducting the study, analyzing the data, and drafting and revising the manuscript*;* L. Saghaei contributed to the conception of the work, analyzing the data*,* and revising the manuscript*;* N. Naghi-Ganji performed the experiments and analyzed the data*;* F. Tavakoli contributed to the molecular docking studies, conducting the study*,* and revising the manuscript*;* V*.* Azimian contributed to the MTT studies and data analysis*,* M*.* Mirian contributed to the conception and supervising*;* H*.* Sirous contributed to molecular docking studies*,* data analysis*,* and supervised these experiments. All authors agreed with all aspects of the work. The final version of the manuscript was approved by all authors.

REFERENCES

1. Siegel RL, Miller KD, Fuchs HE, Jemal A. Cancer statistics, 2021. CA Cancer J Clin. 2021;71(1):7-33. DOI: 10.3322/caac.21654.
2. Wan Y, Li Y, Yan C, Yan M, Tang Z. Indole: a privileged scaffold for the design of anti-cancer agents. Eur J Med Chem. 2019;183:11169. DOI: 10.1016/j.ejmech.2019.111691.
3. Drummond DC, Noble CO, Kirpotin DB, Guo Z, Scott GK, Benz CC. Clinical development of histone deacetylase inhibitors as anticancer agents. Annu Rev Pharmacol Toxicol. 2005;45:495-528. DOI: 10.1146/annurev.phamtox.45.120403.0955825.
4. Sanaei M, Kavoosi F. Histone deacetylases and histone deacetylase inhibitors: molecular mechanisms of action in various cancers. Adv Biomed Res. 2019;8:63-75. DOI: 10.4103/abr.abr_142_19.
5. Choudhary C, Kumar C, Gnad F, Nielsen ML, Rehman M, Walther TC, *et al*. Lysine acetylation targets protein complexes and co-regulates major cellular functions. Science. 2009;325(5942):834-840. DOI: 10.1126/science.1175371.
6. Zhang L, Zhang J, Jiang Q, Zhang L, Song W. Zinc binding groups for histone deacetylase inhibitors. J Enzym Inhib Med Chem. 2018;33(1):714-721. DOI: 10.1080/14756366.2017.1417274.
7. Harshita S, Jaya M, Anjali G. Indole derivatives as potential anticancer agents: a review. J Chil Chem Soc. 2020;65(3):4900-4907. DOI: 10.4067/s0717-97072020000204900.
8. Sahu R, Mishra R, Kumar R, Majee C, Salahuddin, Mazumder A, *et al*. Pyridine moiety: recent advances in cancer treatment. Indian J Pharm Sci. 2021;83(2):162-185. DOI: 10.36468/pharmaceutical-sciences.763.
9. Dai Y, Guo Y, Guo J, Pease LJ, Li J, Marcotte PA, *et al*. Indole amide hydroxamic acids as potent inhibitors of histone deacetylases. Bioorg Med Chem Lett. 2003;13(11):1897-1901. DOI: 10.1016/s0960-894x(03)00301-9.
10. Yang F, Zhao N, Hu Y, Jiang CS, Zhang H. The development process: from SAHA to hydroxamate HDAC inhibitors with branched CAP region and linear linker. Chem Biodivers. 2020;17(1):e1900427. DOI: 10.1002/cbdv.201900427.
11. Cho M, Choi E, Yang JS, Lee C, Seo JJ, Kim BS, *et al*. Discovery of pyridone-based histone deacetylase inhibitors: approaches for metabolic stability. Chem Med Chem. 2013;8(2):272-279. DOI: 10.1002/cmdc.201200529.
12. Frühauf A, Meyer-Almes FJ. Non-hydroxamate zinc-binding groups as warheads for histone deacetylases. Molecules. 2021;26(17):5151. DOI: 10.3390/molecules26175151.
13. Li X, Peterson YK, Inks ES, Himes RA, Li J, Zhang Y, *et al*. Class I HDAC inhibitors display different antitumor mechanism in leukemia and prostatic cancer cells depending on their p53 status. J Med Chem. 2018;61(6):2589-2603. DOI: 10.1021/acs.jmedchem.8b00136.
14. Ning ZQ, Li ZB, Newman MJ, Shan S, Wang XH, Pan DS, *et al*. Chidamide (CS055/HBI-8000): a new histone deacetylase inhibitor of the benzamide class with antitumor activity and the ability to enhance immune cell-mediated tumor cell cytotoxicity. Cancer Chemother Pharmacol. 2012;69(4):901-909. DOI: 10.1007/s00280-011-1766-x.
15. Katner AS. An improved synthesis of indole-3-carboxylic acids. Org Prep Proced. 1970;2(4):297-303. DOI: 10.1080/00304947009458633.
16. Bullock MW, Fox SW. A convenient synthesis of indole-3-acetic acids. J Am Chem Soc. 1951;73(11):5155-51557. DOI: 10.1002/chin.199437104.
17. Hu Y, Ruan W, Gao A, Zhou Y, Gao L, Xu M, *et al*. Synthesis and biological evaluation of novel 4, 5-bisindolyl-1, 2, 4-triazol-3-ones as glycogen synthase kinase-3β inhibitors and neuroprotective agents. Pharmazie. 2017;72(12):707-713. DOI: 10.1691/ph.2017.7722.
18. Song ZL, Zhu Y, Liu JR, Guo SK, Gu YC, Han X, *et al*. Diversity-oriented synthesis and antifungal activities of novel pimprinine derivative bearing a 1, 3, 4-oxadiazole-5-thioether moiety. Mol Divers. 2021;25(1):205-221. DOI: 10.1007/s11030-020-10048-8.
19. Jirousek M, Robert, Paal M, Ruhter G, Schotten T, Takeuchi K, Stenzel W, inventors; VONDRAN-JONES, MaCharri, Agents. Hypoglycemic imidazoline compounds 1999. Publication No. WO/1999/032482. Available from: https://patentscope.wipo.int/search/en/detail.jsf?docId=WO1999032482.

20. Ma Y, Luo W, Quinn PJ, Liu Z, Hider RC. Design, synthesis, physicochemical properties, and evaluation of novel iron chelators with fluorescent sensors. J Med Chem. 2004;47(25):6349-6362. DOI: 10.1021/jm049751s.
21. Zhao DY, Zhang MX, Dong XW, Hu YZ, Dai XY, Wei X, *et al*. Design and synthesis of novel hydroxypyridinone derivatives as potential tyrosinase inhibitors. Bioorg Med Chem Lett. 2016;26(13):3103-3108. DOI: 10.1016/j.bmcl.2016.05.006.
22. Saghaie L, Pourfarzam M, Fassihi A, Sartippour B. Synthesis and tyrosinase inhibitory properties of some novel derivatives of kojic acid. Res Pharm Sci. 2013;8(4):233-242. PMID: 24082892.
23. Mohammadpour M, Sadeghi A, Fassihi A, Saghaei L, Movahedian A, Rostami M. Synthesis and antioxidant evaluation of some novel *ortho*-hydroxypyridine-4-one iron chelators. Res Pharm Sci. 2012;7(3):171-179. PMID: 23181095.
24. Meerloo JV, Kaspers GJ, Cloos J. Cell sensitivity assays: the MTT assay. Methods Mol Biol. 2011;731:237-245. DOI: 10.1007/978-1-61779-080-5_20.
25. Biasini M, Bienert S, Waterhouse A, Arnold K, Studer G, Schmidt T, *et al*. SWISS-MODEL: modelling protein tertiary and quaternary structure using evolutionary information. Nucleic Acids Res. 2014;42(Web Server issue):W252-W258. DOI: 10.1093/nar/gku340.
26. Lagorce D, Bouslama L, Becot J, Miteva MA, Villoutreix BO. FAF-Drugs4: free ADME-tox filtering computations for chemical biology and early stages drug discovery. Bioinformatics. 2017;33(22):3658-3660. DOI: 10.1093/bioinformatics/btx491.
27. O'Boyle NM, Banck M, James CA, Morley C, Vandermeersch T, Hutchison GR. Open Babel: an open chemical toolbox. J Cheminform. 2011;3(1):33,1-14. DOI: 10.1186/1758-2946-3-33.
28. Trott O, Olson AJ. AutoDock Vina: improving the speed and accuracy of docking with a new scoring function, efficient optimization, and multithreading. J Comput Chem. 2010;31(2):455-461. DOI: 10.1002/jcc.21334.
29. Dallakyan S, Olson AJ. Small-molecule library screening by docking with PyRx. Methods Mol Biol. 2015;1263:243-250. DOI: 10.1007/978-1-4939-2269-7_19.
30. Vickers CJ, Olsen CA, Leman LJ, Ghadiri MR. Discovery of HDAC inhibitors that lack an active site Zn^{2+}-binding functional group. ACS Med Chem Let. 2012;3(6):505-508. DOI: 10.1021/ml300081u.
31. Irto A, Cardiano P, Cataldo S, Chand K, Maria Cigala R, Crea F, *et al*. Speciation studies of bifunctional 3-hydroxy-4-pyridinone ligands in the presence of Zn^{2+} at different ionic strengths and temperatures. Molecules. 2019;24(22):4084-4113. DOI: 10.3390/molecules24224084.
32. Saji S, Kawakami M, Hayashi S, Yoshida N, Hirose M, Horiguchi S, *et al*. Significance of HDAC6 regulation *via* estrogen signaling for cell motility and prognosis in estrogen receptor-positive breast cancer. Oncogene. 2005;24(28):4531-4539. DOI: 10.1038/sj.onc.1208646.
33. Huang M, Zhang J, Yan C, Li X, Zhang J, Ling R. Small molecule HDAC inhibitors: promising agents for breast cancer treatment. Bioorg Chem. 2019;91:103184. DOI: 10.1016/j.bioorg.2019.103184.
34. Ding J, Liu J, Zhang Z, Guo J, Cheng M, Wan Y, *et al*. Design, synthesis and biological evaluation of coumarin-based N-hydroxycinnamamide derivatives as novel histone deacetylase inhibitors with anticancer activities. Bioorg Chem. 2020;101:104023. DOI: 10.1016/j.bioorg.2020.104023.
35. Bingul M, Tan O, Gardner CR, Sutton SK, Arndt GM, Marshall GM, *et al*. Synthesis, characterization and anticancer activity of hydrazide derivatives incorporating a quinoline moiety. Molecules. 2016;21(7):916-935. DOI: 10.3390/molecules21070916.
36. Margueron R, Licznar A, Lazennec G, Vignon F, Cavaillès V. Oestrogen receptor alpha increases p21(WAF1/CIP1) gene expression and the antiproliferative activity of histone deacetylase inhibitors in human breast cancer cells. J Endocrinol. 2003;179(1):41-53. DOI: 10.1677/joe.0.1790041.
37. Im JY, Park H, Kang KW, Choi WS, Kim HS. Modulation of cell cycles and apoptosis by apicidin in estrogen receptor (ER)-positive and-negative human breast cancer cells. Chem Biol Interact. 2008;172(3):235-244. DOI: 10.1016/j.cbi.2008.01.007.
38. Yari H, Ganjalikhany MR, Sadegh H. *In silico* investigation of new binding pocket for mitogen activated kinase kinase (MEK): development of new promising inhibitors. Comput Biol Chem. 2015;59 Pt A:185-198. DOI: 10.1016/j.compbiolchem.2015.09.013.
39. Lauffer BEL, Mintzer R, Fong R, Mukund S, Tam C, Zilberleyb I, *et al*. Histone deacetylase (HDAC) inhibitor kinetic rate constants correlate with cellular histone acetylation but not transcription and cell viability. J Biol Chem. 2013;288(37):26926-26943. DOI: 10.1074/jbc.m113.490706.